

tions of the radiocarpal joint with the primary axis of rotation of the midcarpal joint at the neutral position of the wrist.

#### Statistical Analysis

All data were expressed as the mean and standard deviation. Statistical analysis of differences was performed with use of the Student *t* test, with  $p < 0.05$  considered to be significant.

#### Results

##### Direction of Global Wrist Motion

The angles between the direction of the global wrist motion and the wrist flexion-extension axis in the axial plane were  $59^\circ \pm 9^\circ$  in the dart-throwing motion and  $91^\circ \pm 8^\circ$  in the flexion-extension motion. Of the twelve wrists studied in flexion-extension motion, four showed an angle of  $<90^\circ$  (mean,  $82^\circ \pm 4^\circ$ ;

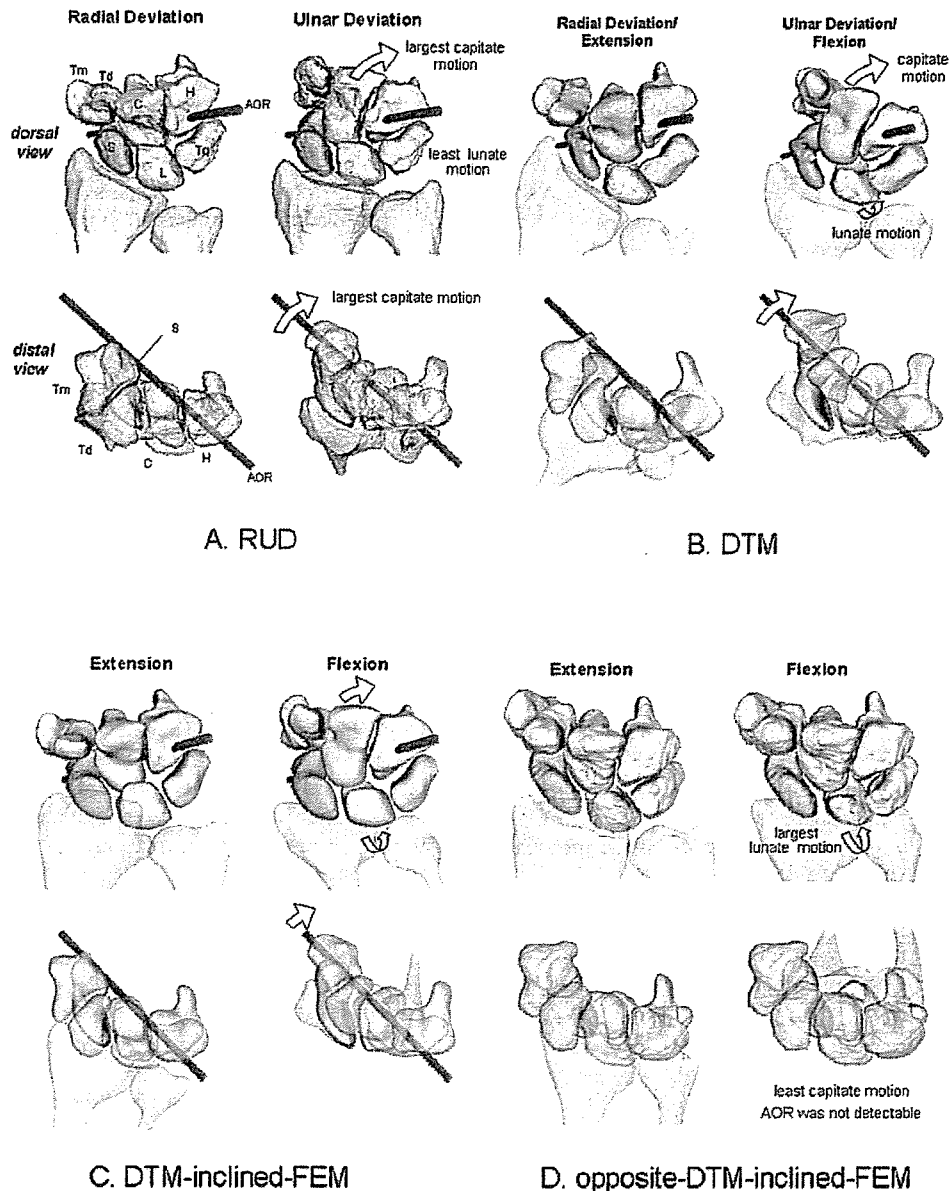


Fig. 1

Dorsal and distal views of the scaphoid-based motions of the right wrist and the axes of rotation (AOR) of the capitate relative to the scaphoid. A: Radioulnar deviation (RUD). B: Dart-throwing motion (DTM). C: Dart-throwing-motion-inclined flexion-extension motion (FEM), and D: opposite-dart-throwing-motion-inclined flexion-extension motion. The amount of motion is related to the length of the arrows. S = scaphoid, L = lunate, Tq = triquetrum, Tm = trapezium, Td = trapezoid, C = capitate, and H = hamate. (See Appendix for accompanying video.)

TABLE 1 Kinematic Data During Dart-Throwing Motion

Case	Age (yr)	Gender	Angle to Axis for Wrist Flexion and Extension (deg)					
			Direction of Global Wrist Motion	Axis of Rotation of Capitate to Scaphoid	Axis of Rotation of Capitate to Lunate	Axis of Rotation of Capitate to Triquetrum	Axis of Rotation of Scaphoid to Radius	Axis of Rotation of Lunate to Radius
1	26	M	55	33	23	21	20	68
2	30	M	56	45	38	35	49	81
3	27	M	57	61	32	43	14	18
4	25	F	58	32	20	21	2	8
5	30	M	69	29	20	6	32	54
6	24	M	69	37	26	27	6	13
7	32	M	66	35	17	17	21	32
8	25	M	73	33	13	14	3	20
9	32	M	43	23	6	12	36	65
10	21	F	47	37	36	24	59	80
11	25	M	56	42	18	8	24	63
12	20	F	62	48	35	13	8	24
Average			59	38	23	20	23	44
Stand. dev.			9	10	10	11	18	27

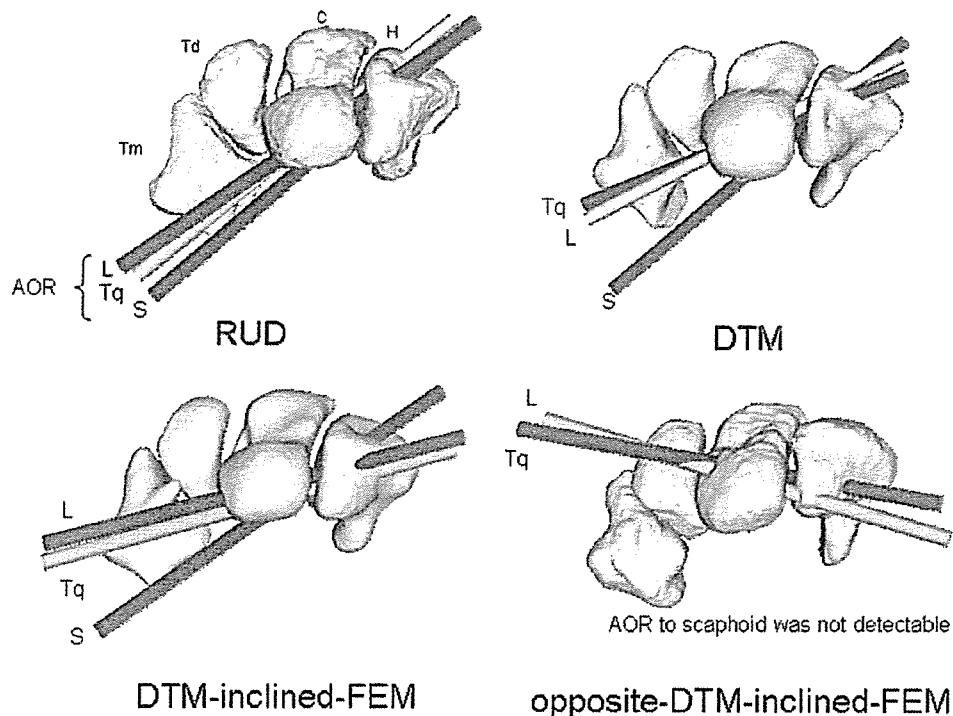


Fig. 2

Proximal view of the distal row of the right wrist and the axes of rotation (AOR) of the capitate relative to the scaphoid (S), lunate (L), and triquetrum (Tq) during radioulnar deviation (RUD), the dart-throwing motion (DTM), the dart-throwing-motion-inclined flexion-extension motion (FEM), and opposite-dart-throwing-motion-inclined flexion-extension motion. Tm = trapezium, Td = trapezoid, C = capitate, and H = hamate.

TABLE 1 (continued)

Range of Motion Around Axis of Rotation (deg)						
Capitate to Scaphoid	Capitate to Lunate	Capitate to Triquetrum	Scaphoid to Lunate	Triquetrum to Lunate	Scaphoid to Radius	Lunate to Radius
59	76	60	20	19	26	12
37	48	40	12	11	28	20
29	35	27	15	9	65	51
27	74	66	47	8	75	27
30	46	30	17	18	33	25
31	40	33	11	8	26	15
40	44	44	18	11	37	30
39	66	55	32	11	54	27
42	67	53	30	15	63	38
28	37	37	9	9	19	11
35	61	46	32	18	47	25
50	58	41	14	26	33	21
37	54	44	21	14	42	25
10	14	12	11	6	18	11

range, 78° to 87°), which means that the plane of global wrist motion inclined slightly toward a dart-throwing-motion plane (the dart-throwing-motion-inclined flexion-extension-motion group). The other eight wrists showed an angle of >90° (mean, 96° ± 4°; range, 91° to 103°), which means that the plane of global wrist motion inclined slightly toward an opposite-dart-throwing-motion plane (the opposite-dart-throwing-motion-inclined flexion-extension-motion group).

#### Midcarpal Motion

##### Motion of the Distal Row Relative to the Scaphoid

The scaphoid-based animation showed the direction of capitate motion relative to the scaphoid to be always similar: it was oblique and it extended from radiodorsal to ulnopalmar in radioulnar deviation, in the dart-throwing motion, and in the dart-throwing-motion-inclined flexion-extension motion. From wrist radial deviation, radial deviation/extension, or extension to wrist ulnar deviation, ulnar deviation/flexion, or flexion, respectively, the capitate always moved from radiodorsal to ulnopalmar (Fig. 1, A, B, and C; see Appendix for videos).

The axes of rotation between the scaphoid and capitate in radioulnar deviation, in the dart-throwing motion, and in the dart-throwing-motion-inclined flexion-extension motion were located closely in space and obliquely penetrated the neck of the capitate from a radiopalmar to an ulnodorsal direction. In the axial plane, the axes of rotation of the capitate relative to the scaphoid in radioulnar deviation, in the dart-throwing motion, and in the dart-throwing-motion-inclined flexion-extension motion formed a radially and palmarly opening angle of 43° ± 7° (as previously reported<sup>7</sup>), 38° ± 10°,

and 31° ± 9°, respectively, with the wrist flexion-extension axis (Tables I and II). There were no significant differences between these angles.

In the opposite-dart-throwing-motion-inclined flexion-extension motion, the capitate seldom moved and the scapho-trapezotrapezoid joint appeared to be "locked" (Fig. 1, D; see Appendix for videos). The axes of rotation between the scaphoid and capitate in the opposite-dart-throwing-motion-inclined flexion-extension motion varied considerably (mean angle with the wrist flexion-extension axis, 5° ± 53°) so that a consistent pattern of the axis of rotation was not detectable. In some wrists (Cases 20 and 24), the intercarpal joints between the trapezium, trapezoid, and capitate showed irregular motions; the trapezium and trapezoid translated distalward relative to the trapezoid and capitate, respectively, when the wrist moved from extension to flexion.

As the global wrist motion changed from radioulnar deviation to the opposite-dart-throwing-motion-inclined flexion-extension motion, the range of the capitate rotation relative to the scaphoid gradually decreased. The ranges of rotation of the capitates around their own axes of rotation were 41° ± 10° in radioulnar deviation (as previously reported<sup>7</sup>), 37° ± 10° in the dart-throwing motion, 27° ± 5° in the dart-throwing-motion-inclined flexion-extension motion, and 9° ± 15° in the opposite-dart-throwing-motion-inclined flexion-extension motion (Tables I and II). There were significant differences between the values in radioulnar deviation and the dart-throwing-motion-inclined flexion-extension motion ( $p < 0.05$ ), between those in the dart-throwing motion and the dart-throwing-motion-inclined flexion-extension motion ( $p < 0.05$ ), and between those in the dart-throwing-motion-inclined

TABLE II Kinematic Data During Flexion-Extension Motion

Wrist Motion/Case	Age (yr)	Gender	Direction of Global Wrist Motion	Angle to Axis for Wrist Flexion and Extension (deg)				
				Axis of Rotation of Capitate to Scaphoid	Axis of Rotation of Capitate to Lunate	Axis of Rotation of Capitate to Triquetrum	Axis of Rotation of Scaphoid to Radius	Axis of Rotation of Lunate to Radius
<b>Dart-throwing-motion-inclined flexion-extension motion</b>								
13	30	M	78	21	18	11	6	5
14	24	M	80	40	16	18	1	-3
15	27	M	87	25	2	0	-8	1
16	24	F	84	38	17	28	-2	-1
Average			82	31	13	14	-1	1
Stand. dev.			4	9	7	12	6	3
<b>Opposite-dart-throwing-motion-inclined flexion-extension motion</b>								
17	25	F	92	-14	-1	-13	8	12
18	26	M	95	-25	-15	3	0	1
19	30	M	99	-54	-19	-20	-5	-12
20	24	M	103	87	-59	-31	-8	2
21	32	M	91	-2	-3	0	0	0
22	20	F	92	-48	-16	-22	-8	-8
23	21	F	96	16	-12	-22	-2	-5
24	25	M	98	78	-22	-24	0	-2
Average			96	5	-18	-16	-2	-2
Stand. dev.			4	53	18	12	5	7
Total average			91	14	-8	-6	-2	-1
Stand. dev. for total average			8	45	21	19	5	6

flexion-extension motion and the opposite-dart-throwing-motion-inclined flexion-extension motion ( $p < 0.05$ ).

#### Motion of the Distal Row Relative to the Lunate and Triquetrum

When the global wrist motion changed from radioulnar deviation to the opposite-dart-throwing-motion flexion-extension motion, the directions of the capitate motions relative to the lunate and triquetrum inclined in a similar way, which was clearly different from the capitate motion relative to the scaphoid. The capitate motions relative to the lunate and triquetrum in the midcarpal joint were essentially similar and synchronous with each other regardless of the type of wrist motion.

The axes of rotation of the capitate relative to the lunate and triquetrum in the dart-throwing motion and flexion-extension motion ran more transversely in the axial plane than did those during radioulnar deviation (Fig. 2). The axes of rotation of the capitate relative to the lunate and triquetrum formed, with the wrist flexion-extension axis, a radially and palmarly opening angle of  $41^\circ \pm 11^\circ$  and  $42^\circ \pm 14^\circ$ , respectively, in radioulnar deviation (previously reported<sup>7</sup>),  $23^\circ \pm 10^\circ$  and  $20^\circ \pm 11^\circ$  in the dart-throwing motion,  $13^\circ \pm 7^\circ$  and  $14^\circ \pm 12^\circ$  in the dart-throwing-motion-inclined flexion-extension mo-

tion, and  $-18^\circ \pm 18^\circ$  and  $-16^\circ \pm 12^\circ$  in the opposite-dart-throwing-motion-inclined flexion-extension motion (Tables I and II). There were significant differences in the values between radioulnar deviation and the dart-throwing motion ( $p < 0.0005$ ), between radioulnar deviation and the dart-throwing-motion-inclined flexion-extension motion ( $p < 0.0005$ ), and between the dart-throwing-motion-inclined flexion-extension motion and the opposite-dart-throwing-motion-inclined flexion-extension motion ( $p < 0.005$ ).

The ranges of motion of the capitate relative to the lunate and triquetrum around their own axes of rotations were  $44^\circ \pm 10^\circ$  and  $33^\circ \pm 6^\circ$ , respectively, in radioulnar deviation (as previously reported<sup>7</sup>),  $54^\circ \pm 14^\circ$  and  $44^\circ \pm 12^\circ$  in the dart-throwing motion,  $48^\circ \pm 7^\circ$  and  $33^\circ \pm 8^\circ$  in the dart-throwing-motion-inclined flexion-extension motion, and  $41^\circ \pm 12^\circ$  and  $38^\circ \pm 9^\circ$  in the opposite-dart-throwing-motion-inclined flexion-extension motion (Tables I and II). The values did not differ significantly among the different types of wrist motion.

#### Global Capitate-Based Midcarpal Motion

Regardless of the type of wrist motion, the animation of the capitate-based midcarpal motion showed that the loci of the displacement of all of the joint surfaces of the midcarpal joint

TABLE II (continued)

Range of Motion Around Axis of Rotation (deg)						
Capitate to Scaphoid	Capitate to Lunate	Capitate to Triquetrum	Scaphoid to Lunate	Triquetrum to Lunate	Scaphoid to Radius	Lunate to Radius
26	55	43	30	13	77	47
22	39	25	21	15	77	56
34	51	34	26	21	91	68
27	47	29	24	19	84	60
27	48	33	25	17	82	58
5	7	8	4	4	7	9
17	61	54	45	13	83	38
21	47	41	26	13	69	43
20	37	40	23	8	80	58
-12	23	28	16	17	61	47
18	47	38	33	15	99	70
15	44	42	33	11	124	75
5	29	24	24	16	76	53
-16	38	38	33	9	86	53
9	41	38	29	13	84.75	55
15	12	9	9	3	19	13
15	43	36	28	14	84	56
15	11	9	8	4	16	1

were located within a midcarpal ovoid space whose major axis coincided with the typical axis of rotation of the scaphoid, running from a radiopalmar to an ulnodorsal direction (Figs. 3 and 4; see Appendix for videos). A line connecting the centers of the joint surfaces of the midcarpal joint could be schematized as a letter "C" entwining the midcarpal ovoid (Figs. 3, B, and 5, A).

We also found a specific pattern of midcarpal motion for each wrist motion (Fig. 4). We previously showed that the directions and ranges of motion of the lunate and triquetrum were not significantly different from those of the scaphoid in radioulnar deviation<sup>7</sup>. In the dart-throwing motion, the directions of the lunate and triquetrum slightly inclined toward a wrist flexion-extension-motion plane and the ranges of motion did not change significantly compared with those in radioulnar deviation, while the direction of the scaphoid motion was not significantly different from that in radioulnar deviation but the range of scaphoid motion decreased. When the wrist was moved in a dart-throwing-motion-inclined flexion-extension-motion plane, these tendencies became more pronounced: the directions of the lunate and triquetrum inclined more, while the range of scaphoid motion decreased more. Finally, when the wrist was moved in an opposite-dart-throwing-motion-inclined flexion-extension-motion plane,

the scaphoid seldom moved but the lunate and triquetrum moved along the plane of the scapholunate joint, with the range of motion not significantly changing. The lunate and triquetrum always moved separately, but the directions of the motions of the lunocapitate and triquetrohamate joints were not significantly different from each other.

In summary, as the global wrist motion changed from radioulnar deviation to the opposite-dart-throwing-motion flexion-extension motion, the range of motion of the scaphoid in the midcarpal joint gradually decreased without the direction changing significantly and the ranges of motion of the lunate and triquetrum did not significantly change but the direction gradually inclined from a dart-throwing-motion plane to an opposite-dart-throwing-motion-inclined flexion-extension-motion plane.

#### *Motion Between the Scaphoid and Lunate and Between the Lunate and Triquetrum*

The scaphoid-based animation showed that as the wrist moved from radial deviation, radial deviation/extension, or extension to ulnar deviation, ulnar deviation/flexion, or flexion, respectively, the lunate always rotated dorsally relative to the scaphoid; the relative position between the scaphoid and lunate was similar to the dorsiflexed intercalated segment insta-

bility posture (Fig. 1; see Appendix for videos).

As the global wrist motion changed from radioulnar deviation to the opposite-dart-throwing-motion-inclined flexion-extension motion, the range of rotation of the lunate relative to the scaphoid gradually increased, averaging  $8^\circ \pm 6^\circ$  in radioulnar deviation (as previously reported<sup>7</sup>),  $21^\circ \pm 11^\circ$  in the dart-throwing motion,  $25^\circ \pm 4^\circ$  in the dart-throwing-motion-inclined flexion-extension motion, and  $29^\circ \pm 9^\circ$  in the opposite-dart-throwing-motion-inclined flexion-extension motion (Tables I and II). There was a significant difference in the values between radioulnar deviation and the dart-throwing motion ( $p < 0.001$ ), radioulnar deviation and the dart-throwing-motion-inclined flexion-extension motion ( $p < 0.0001$ ), and radioulnar deviation and the opposite-dart-throwing-motion-inclined flexion-extension motion ( $p < 0.0001$ ).

The lunotriquetral joint also moved in all types of wrist motion; however, we did not find a significant difference in the range of motion of the triquetrum relative to the lunate between radioulnar deviation, dart-throwing motion, and flexion-extension motion (Tables I and II).

#### Relationship Between Midcarpal and Radiocarpal Kinematics

The axes of rotation of the scaphoid and lunate relative to the radius were almost parallel to each other and passed through

the neck of the capitate in all types of wrist motion. The relationship between the major axis of the midcarpal ovoid and the wrist flexion-extension axis was opposite the relationship between the axes of the radiocarpal joint and the wrist flexion-extension axis in radioulnar deviation, the relationships were similar in the dart-throwing motion, and the relationships were midway between those in radioulnar deviation and the dart-throwing motion in the flexion-extension motion.

In the axial plane, the axes of rotation of the scaphoid and lunate relative to the radius formed radially and palmarly opening angles with the wrist flexion-extension axis of  $-43^\circ \pm 20^\circ$  and  $-39^\circ \pm 14^\circ$ , respectively, in radioulnar deviation (as previously reported<sup>7</sup>);  $23^\circ \pm 18^\circ$  and  $44^\circ \pm 27^\circ$  in the dart-throwing motion;  $-1^\circ \pm 6^\circ$  and  $1^\circ \pm 3^\circ$  in the dart-throwing-motion-inclined flexion-extension motion; and  $-2^\circ \pm 5^\circ$  and  $-2^\circ \pm 7^\circ$  in the opposite-dart-throwing-motion-inclined flexion-extension motion (Tables I and II). There were significant differences in these values between radioulnar deviation and the dart-throwing motion ( $p < 0.0001$ ) and between the dart-throwing motion and the dart-throwing-motion-inclined flexion-extension motion ( $p < 0.05$ ).

#### Discussion

We previously investigated the scaphotrapeziotrapezoid joint in cadavers both anatomically<sup>12</sup> and kinemati-

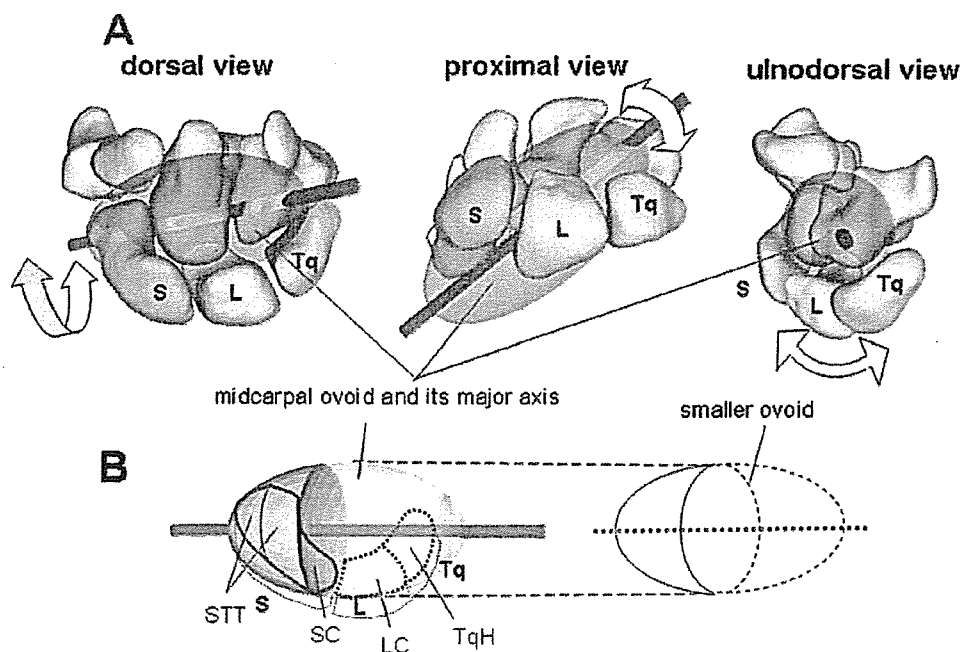


Fig. 3

A: Dorsal, proximal, and ulnodorsal views of the right carpus and a superimposed midcarpal ovoid, the major axis of which coincides with the typical axis of rotation of the scaphoid relative to the capitate. S = scaphoid, L = lunate, and Tq = triquetrum. B: A schematic of the dorsodistal view of the midcarpal ovoid with which the scaphotrapeziotrapezoid (STT), lunocapitate (LC), and triquetrohamate (TqH) joints come into contact. The scaphocapitate (SC) joint comes into contact with a smaller ovoid, the axis of which coincides with the major axis of the midcarpal ovoid.

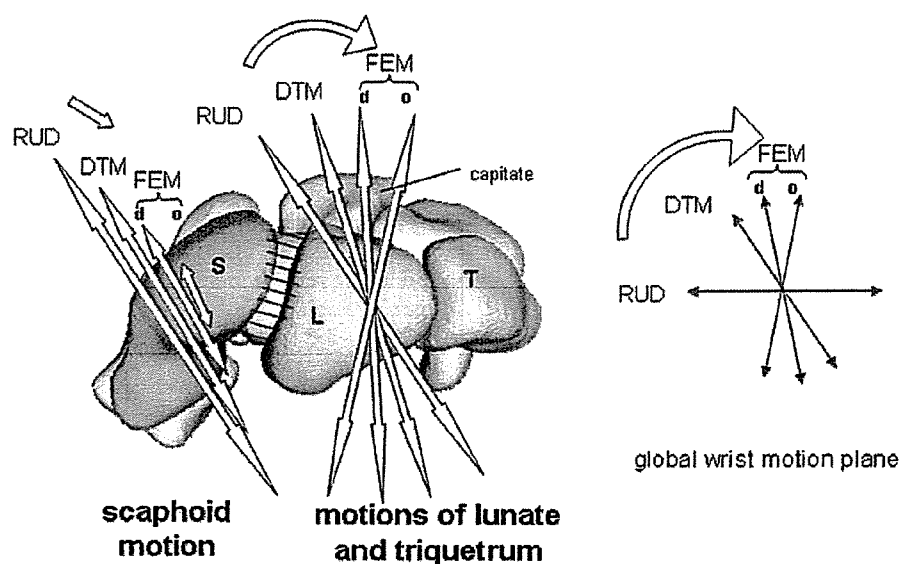


Fig. 4

Proximal view of the right carpus, showing the direction and range of motions of the scaphoid (S), lunate (L), and triquetrum (T) relative to the capitate in radioulnar deviation (RUD), the dart-throwing motion (DTM), the dart-throwing-motion-inclined flexion-extension motion (FEM) (d), and the opposite-dart-throwing-motion-inclined flexion-extension motion (o). The amount of motion is related to the length of the arrows. (See Appendix for accompanying video.)

cally<sup>15</sup>, and those studies suggested that the scaphotrapezotrapezoid joint has essentially a single degree of freedom, or is a uniaxial joint. The results of this current in vivo kinematic study further revealed that the range of motion of the scaphoid in the midcarpal joint gradually decreases as the global wrist motion changes from radioulnar deviation to flexion-extension motion. We noticed that the convex joint surfaces of the scaphoid articulating with the trapezium and the trapezoid can approximate an ovoid whose major axis runs from a radiopalmar to an ulnodorsal direction and coincides with the axis of rotation of the capitate relative to the scaphoid. Moreover, the concave joint surface of the scaphoid articulating with the capitate can also be a part of a smaller ovoid whose axis is the same as the major axis of the midcarpal ovoid (Fig. 3, B). Actually, the axis of rotation of the joint between the scaphoid and the distal carpal row is not rigid, probably because of minor mobility occurring among the trapezium, trapezoid, and capitate<sup>14</sup> and a lack of ligamentous constraint between the proximal part of the scaphoid and the capitate. Thus, this joint is essentially uniaxial, but it also has an adaptive mechanism that allows preservation of articular congruity of the midcarpal joint when distortional force is applied.

We have also found that the skeletal constraint of the triquetrohamate joint is relatively weak because the joint is essentially an ellipsoidal joint with two degrees of freedom, or is a biaxial joint<sup>8</sup>. The current study further revealed that the motion of the lunate was always similar to that of the triquetrum. Our three-dimensional analysis showed that most of the joint surfaces of the lunocapitate and triquetrohamate

joints are also part of the midcarpal ovoid whose major axis runs in a radiopalmar to an ulnodorsal direction (Fig. 3, B). Thus, most of the joint surfaces in the midcarpal joint are contained within a midcarpal ovoid; the carpal bones might be moving within this volume, but they still have distinct motions relative to each other within it.

We consider midcarpal motion to be essentially the combined motion of three types of joint systems: (1) the uniaxial joint between the scaphoid and the distal row, the axis of which runs in a radiopalmar to an ulnodorsal direction; (2) the biaxial and ellipsoidal joint between the lunate and triquetrum and the distal row; and (3) the intercarpal joints of the proximal row, which have an adaptive mechanism that accommodates the above-mentioned two types of joint systems in the midcarpal joint. We believe that the primary motion plane in the midcarpal joint is a dart-throwing plane, which is defined by anatomical constraints of the joint between the scaphoid and the distal row; however, adaptive intercarpal motions, mainly in the scapholunate joint, and relatively weak constraints of the lunocapitate and triquetrohamate joints allow the global midcarpal joint to move in the flexion-extension or even the opposite-dart-throwing-motion-inclined flexion-extension-motion planes as well.

This study raises concerns about a self-stabilizing mechanism of the carpus under load. When the trapezium is axially loaded against the scaphoid, the scaphoid tends to rotate into flexion; this flexion moment is constrained by the extension moment experienced by the triquetrum, and stable equilibrium is achieved<sup>15,16</sup>. As a modification of this concept, we ad-

vocate use of an “ovoid/C” concept to explain the carpal self-stabilizing mechanism. The three-dimensional configuration of a line connecting the centers of the joint surfaces of the midcarpal joint can be schematized as a letter “C” entwining a midcarpal ovoid (Figs. 3, B, and 5, A). On the radiograph of a semisupinated wrist (Fig. 5, B), which is almost compatible with an axial radiograph of the ovoid, the midcarpal joint displays a C-shaped outline<sup>7</sup>. The ulnopalmar rotational moment of the scaphoid generated by the inclination of both the scaphotrapeziotrapezoid and the scaphocapitate joint competes and maintains balance with the radiodorsal rotational moment of the triquetrum generated by the inclination of the triquetrohamate joint (Fig. 5, B). Gilula and Weeks reported that three fairly smooth radiographic arcs can be drawn to define the normal carpal relationship, and disruption of any one of these lines may indicate a major carpal derangement<sup>7</sup>. We believe that our C-shaped outline on the radiograph of a semisupinated wrist could provide additional information about carpal derangement because this view is

essentially a lateral view of the midcarpal joint.

In terms of the kinematic relationship between the midcarpal joint and the radiocarpal joint, the question arises of how the oblique midcarpal motion accommodates itself to radiocarpal motion. It is well known that, during radioulnar deviation, the three proximal carpal bones move synergistically relative to the radius from a flexed and radially deviated position in wrist radial deviation to an extended and ulnarly deviated position in wrist ulnar deviation<sup>5,18-20</sup>. This finding is consistent with our observation that the axes of rotation of the proximal row relative to the radius run in a radiodorsal to an ulnopalmar direction. The relationship between the primary axes of the midcarpal joint and the radiocarpal joint during radioulnar deviation is reciprocal, effectively canceling rotation in the flexion-extension plane of the hand on the forearm. During the dart-throwing motion, the axes of the two joints are similar and synergistic with each other, which may explain why the range of wrist motion achieved in this plane is greater than that achieved in radioulnar deviation and why the dart-throwing plane is the usual

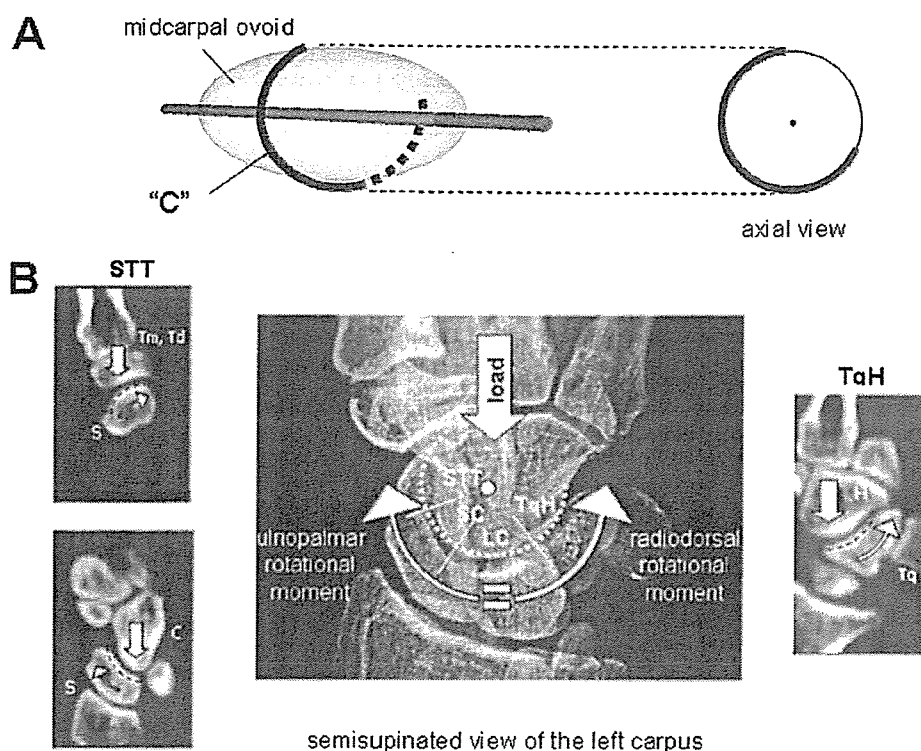


Fig. 5


The “ovoid/C” concept. A: The three-dimensional configuration of a line connecting the centers of the joint surfaces of the midcarpal joint can be schematized as a letter “C” entwining a midcarpal ovoid. The “C” clearly appears to form a three-quarter circle in the axial view of the ovoid. B: Semisupinated radiograph of the left carpus, which is compatible with an axial view of the ovoid of the right carpus, and the tomograms at the level of the scaphotrapeziotrapezoid (STT), scaphocapitate (SC), and triquetrohamate (TqH) joints. In this plane, the midcarpal joint displays a C-shaped outline, and the ulnopalmar rotational moment of the scaphoid generated by the inclination of the scaphotrapeziotrapezoid and scaphocapitate joints maintains balance with the radiodorsal rotational moment of the triquetrum generated by the inclination of the triquetrohamate joint.



plane of utilization of the wrist<sup>21</sup>. During flexion-extension motion, the axis of the radiocarpal joint is almost the same as the wrist flexion-extension axis and the axis of the midcarpal joint is oblique, findings that are consistent with the fact that, normally, extension of the wrist is associated with radial deviation and flexion is associated with ulnar deviation<sup>18</sup>.

Our current kinematic technique has some limitations, the greatest of which is that the study was based on static three-dimensional views of the carpus in the limited number of wrist positions examined. The static measurement does not include any inertial or functional effects that might occur during normal wrist motion. The angles of the axis of rotation would not be fixed angles for the entire range of motion; they would have varied if we had used more increments of motion. It would be reasonable to perform dynamic studies to supplement this study. We tried to establish the wrist dart-throwing motion as an oblique wrist motion relative to the sagittal plane, but there is no consensus about what constitutes the true plane of the wrist dart-throwing motion<sup>22</sup>. However, the technique that we used in this study allowed us to obtain new information on in vivo three-dimensional midcarpal kinematics without subjecting the volunteers to radioactive exposure. Our findings suggest that the proximal carpal row with all its related joints has a unique mechanism that contributes to both the stability and the mobility of the wrist. Hopefully, this new information on the ovoid/C-shape perspective of the anatomy and the kinematics of the midcarpal joint will assist clinicians in obtaining a better understanding of the wrist joint and some of its disorders.

## Appendix

 Videos of the midcarpal motions (as supplements to Figures 1 and 4) are available on our web site at [jbjs.org](http://jbjs.org) (go to the article citation and click on "Supplementary Material"). ■

Hisao Moritomo, MD  
Tsuyoshi Murase, MD  
Akira Goto, MD  
Kunihiko Oka, MD  
Kazuomi Sugamoto, MD  
Hideki Yoshikawa, MD, PhD

Department of Orthopaedic Surgery, Osaka University, 2-2 Yamadaoka, Suita-shi, Osaka 565-0871, Japan. E-mail address for H. Moritomo: [moritomo@ort.med.osaka-u.ac.jp](mailto:moritomo@ort.med.osaka-u.ac.jp)

In support of their research for or preparation of this manuscript, one or more of the authors received Grants-in-Aid for Scientific Research, the Ministry of Education, Science and Culture in Japan, and Grant of Japan Orthopaedics and Traumatology Foundation, Inc. (No. 0146). None of the authors received payments or other benefits or a commitment or agreement to provide such benefits from a commercial entity. No commercial entity paid or directed, or agreed to pay or direct, any benefits to any research fund, foundation, educational institution, or other charitable or nonprofit organization with which the authors are affiliated or associated.

doi:10.2106/JBJS.D.02885

## References

- Kobayashi M, Berger RA, Linscheid RL, An KN. Intercarpal kinematics during wrist motion. *Hand Clin*. 1997;13:143-9.
- de Lange A, Kauer JM, Hulskes R. Kinematic behavior of the human wrist joint: a roentgen-stereophotogrammetric analysis. *J Orthop Res*. 1985;3:56-64.
- Ruby LK, Cooney WP 3rd, An KN, Linscheid RL, Chao EY. Relative motion of selected carpal bones: a kinematic analysis of the normal wrist. *J Hand Surg [Am]*. 1988;13:1-10.
- Savelberg HH, Otten JD, Kooloos JG, Hulskes R, Kauer JM. Carpal bone kinematics and ligament lengthening studied for the full range of joint movement. *J Biomech*. 1993;26:1389-402.
- Kauer JM. The interdependence of carpal articulation chains. *Acta Anat (Base)*. 1974;88:481-501.
- Seradge H, Sterbank PT, Seradge E, Owens W. Segmental motion of the proximal carpal row: their global effect on the wrist motion. *J Hand Surg [Am]*. 1990;15:236-9.
- Moritomo H, Murase T, Goto A, Oka K, Sugamoto K, Yoshikawa H. Capitate-based kinematics of the midcarpal joint during wrist radioulnar deviation: an in vivo three-dimensional motion analysis. *J Hand Surg [Am]*. 2004;29:668-75.
- Moritomo H, Goto A, Sato Y, Sugamoto K, Murase T, Yoshikawa H. The triquetrum-hamate joint: an anatomic and in vivo three-dimensional kinematic study. *J Hand Surg [Am]*. 2003;28:797-805.
- Goto A, Moritomo H, Murase T, Oka K, Sugamoto K, Arimura T, Nakajima Y, Yamazaki T, Sato Y, Tamura S, Yoshikawa H, Ochi T. In vivo elbow biomechanical analysis during flexion: three-dimensional motion analysis using magnetic resonance imaging. *J Shoulder Elbow Surg*. 2004;13:441-7.
- Patterson RM, Nicodemus CL, Viegas SF, Elder KW, Rosenblatt J. High-speed, three-dimensional kinematic analysis of the normal wrist. *J Hand Surg [Am]*. 1998;23:446-53.
- Panjabi MM, Krag MH, Goel VK. A technique for measurement and description of three-dimensional six degree-of-freedom motion of a body joint with an application to the human spine. *J Biomech*. 1981;14:447-60.
- Moritomo H, Viegas SF, Nakamura K, Dasilva MF, Patterson RM. The scaphotrapezio-trapezoidal joint. Part 1: an anatomic and radiographic study. *J Hand Surg [Am]*. 2000;25:899-910.
- Moritomo H, Viegas SF, Elder K, Nakamura K, Dasilva MF, Patterson RM. The scaphotrapezio-trapezoidal joint. Part 2: a kinematic study. *J Hand Surg [Am]*. 2000;25:911-20.
- Sonenblum SE, Crisco JJ, Kang I, Akelman E. In vivo motion of the scaphotrapezio-trapezoidal (STT) joint. *J Biomech*. 2004;37:645-52.
- Kobayashi M, Garcia-Elias M, Nagy L, Ritt MJ, An KN, Cooney WP, Linscheid RL. Axial loading induces rotation of the proximal carpal row bones around unique screw-displacement axes. *J Biomech*. 1997;30:1165-7.
- Garcia-Elias M, Lluch A. Partial excision of scaphoid: is it ever indicated? *Hand Clin*. 2001;17:687-95, x.
- Gilula LA, Weeks PM. Post-traumatic ligamentous instabilities of the wrist. *Radiology*. 1978;129:641-51.
- Fisk G. Biomechanics of the wrist joint. In: Tubiana R, editor. *The hand*. Philadelphia: WB Saunders; 1981. p 136-41.
- Horii E, Garcia-Elias M, An KN, Bishop AT, Cooney WP, Linscheid RL, Chao EY. A kinematic study of luno-triquetral dissociations. *J Hand Surg [Am]*. 1991;16:355-62.
- Garcia-Elias M. Kinetic analysis of carpal stability during grip. *Hand Clin*. 1997;13:151-8.
- Saffer P, Semaan I. The study of the biomechanics of wrist movements in an oblique plane—a preliminary report. In: An KN, Garcia-Elias M, Cooney WP 3rd, Schulnd F, editors. *Advances in the biomechanics of the hand and wrist*. New York: Plenum Press; 1994. p 305-11.
- Werner FW, Green JK, Short WH, Masaoka S. Scaphoid and lunate motion during a wrist dart throw motion. *J Hand Surg [Am]*. 2004;29:418-22.

# Modulation of Peritendinous Adhesion Formation by Alginate Solution in a Rabbit Flexor Tendon Model

Jiro Namba,<sup>1</sup> Kozo Shimada,<sup>2</sup> Masanobu Saito,<sup>3</sup> Tsuyoshi Murase,<sup>4</sup> Hideaki Yamada,<sup>5</sup> Hideki Yoshikawa<sup>4</sup>

<sup>1</sup> Department of Orthopaedic Surgery, Minoh City Hospital, 5-7-1, Kayano, Minoh, Osaka 562-0014, Japan

<sup>2</sup> Department of Orthopaedic Surgery, Rinku General Medical Center, Izumisano Municipal Hospital, 2-23, Rinku Orai-kita, Izumisano, Osaka 598-0048, Japan

<sup>3</sup> Department of Orthopaedic Surgery, Osaka-minami Medical Center, 2-1, Kidohigashi, Kawachinagano, Osaka 586-0008, Japan

<sup>4</sup> Department of Orthopaedic Surgery, Osaka University Graduate School of Medicine, 2-2, Yamada-oka, Suita, Osaka 565-0871, Japan

<sup>5</sup> Medical Research Group, Kuraray Medical Company, Ltd., 1621, Sakazu, Kurashiki, Okayama 710-8622, Japan

Received 5 March 2005; revised 3 December 2005; accepted 27 February 2006  
Published online 9 June 2006 in Wiley InterScience (www.interscience.wiley.com). DOI: 10.1002/jbm.b.30594

**Abstract:** To examine the antiadhesive effect of an alginate solution following tendon surgery, unilateral subtotal laceration of the flexor digitorum communis tendon was created in one hind limb while the other side was left intact in 32 Japanese white rabbits. The lesion was coated with alginate solution in 16 animals and not coated in the other 16. Degree of adhesion formation was assessed histologically and biomechanically by measuring the flexion angle of the first toe when the flexor digitorum tendon was pulled with a specified force at 4 weeks postoperatively. When compared with the control group, the alginate-treated group demonstrated significantly greater toe flexion, with less scar tissue formation at the repair site. Histologically, complete tendon healing with longitudinal remodeling of collagen fibers was observed in the alginate-treated group, while a random pattern of fibers was observed in the control group. Reduction in adhesion formation using alginate solution represents a novel strategy for the management of tendon injury and repair in the clinical setting. © 2006 Wiley Periodicals, Inc. *J Biomed Mater Res Part B: Appl Biomater* 80B: 273–279, 2007

**Keywords:** alginate; tendon; adhesion; polysaccharide; tendon repair

## INTRODUCTION

Peritendinous adhesion is a major problem following tendon surgery. Adhesions interfere with tendon gliding and restrict tendon excursion, thereby causing poor functional results after tendon repair. Until recently, many investigators considered the tendon to have the ability to heal itself (intrinsic theory) and believed that the extrinsic mechanism, which is an inflammatory response to injury, is not essential to the healing process. A number of methods, most of which use mechanical barriers, including synthetic materials,<sup>1–3</sup> around the repair site, have been applied in order to physically block scar tissue intrusion, but no satisfactory approach has been established to date.

Debate concerning tendon repair has continued and it is now generally accepted that tendons heal by a combination of both intrinsic and extrinsic mechanisms,<sup>4,5</sup> although there seems to be an imbalance between the two mechanisms during the initial phase of tendon healing.<sup>6</sup> During this phase, the extrinsic mechanism predominates over the intrinsic mechanism, the onset of which is delayed. We hypothesized that the best approach to reduce peritendinous adhesion is not to prevent extrinsic mechanisms completely, but to modulate the behavior of extrinsic-derived cells. That is to say, antiadhesive materials should be selectively permeable, allowing permeation of low-molecular-weight nutritional substances, which are essential for the intrinsic mechanism, but not entities at the cell-size level such as fibroblasts and leukocytes that migrate from the extrinsic field.

One such candidate is alginate, an intercellular polysaccharide known to be widely distributed in brown seaweed. Alginate is utilized in immobilizing living cells because of its easy gelation, good biocompatibility, and low toxicity.<sup>7</sup> In

Correspondence to: J. Namba (e-mail: yonamba@ybb.ne.jp or hospital@maple.city.minoh.lg.jp)

© 2006 Wiley Periodicals, Inc.

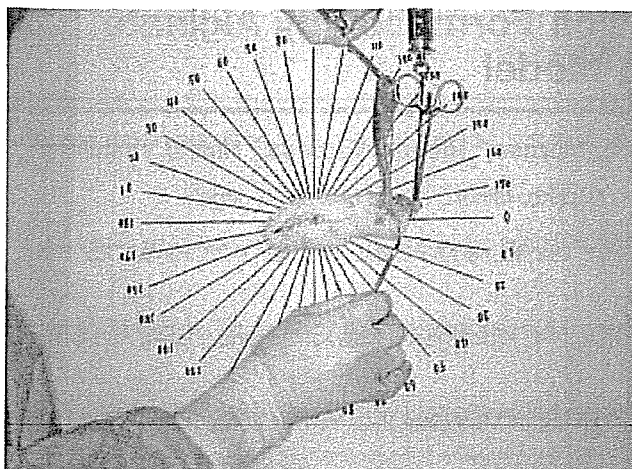


**Figure 1.** The method of mechanical evaluation. The limb was placed in a vertical position with its proximal tibia and calcaneus immobilized by a clamp. The leg was observed from the medial side in front of a white screen bearing radial lines representing a protractor. The first metatarsophalangeal joint was positioned at the center of the protractor. The flexion angle of the first toe was measured at the rest position and when pulled with a 400-g force (measured with a spring-type scale). The flexion range of motion was determined as the difference between the rest position and the flexed position.

allo- and xenogeneic islet transplantation, the best results have been obtained with alginate microcapsules; success in this procedure was attained by enclosing grafts in a selectively permeable alginate membrane.<sup>8</sup> The membrane only allows the permeation of smaller molecules, such as oxygen, glucose and insulin, preventing the penetration of immunocytes and larger immune molecules.<sup>8</sup> We hypothesized that the same cell immobilization effect would occur in the application of alginate to injured tendon. The present study investigated whether a beneficial antiadhesive effect could be obtained using alginate solution on rabbit tendon injury.

## MATERIALS AND METHODS

### Experimental Animals

Thirty-two Japanese white rabbits weighing around 3000 g were used. All rabbits were free of disease, and each experimental procedure was approved by the Committee on the Use and Care of Animals of Kuraray Co..

### Preparation of Alginate Solution

Sodium alginate powder used in the experiment was derived from *Lassonia nigrescens* (Kimitsu Chemical Industries, Japan). This substance had the following characteristics as reported by the manufacturer: M/G ( $\beta$ -D-mannuronic acid/ $\alpha$ -L-guluronic acid) ratio, 1.3; weight-average molecular weight,  $M_w/10^4 = 54$ ; and polydispersity index,  $M_w/M_n = 5.43$ . It had a purity of at least 99% and was sterile, but was not specified as being pyrogen-free. However, the Limulus

amebocyte lysate testing showed that the alginate's endotoxin concentration was less than 10 EU/g. When typical concentrations of sodium alginate solution and  $\text{CaCl}_2$  solution are used in cell encapsulation, sodium alginate rapidly forms a hard gel that cannot be applied as a coatable or injectable tendon adhesion barrier gel. To overcome this phenomenon, very high concentrations of sodium alginate were utilized without the crosslinking method. The alginate solution was first adjusted to a concentration of 10% (by weight). Autoclave sterilization at 121°C for 20 min was then done to depolymerize the alginate solution and to reduce the molecular weight to  $2.4\text{--}4.0 \times 10^5 M_w$  (as measured by high-speed liquid chromatography, Waters Alliance, Waters, Japan). Final processed alginate solution remained 10% concentrated and was adequately viscous for injection and coating.

### Surgical Procedure

Full-thickness lacerations were used in a preliminary study; however, when this was performed, tendons were ruptured or

**TABLE I.** Flexion Angle Percentage<sup>a</sup>

Animal Number	Flexion Angle (%)
Alginate-treated group	
1	87.5
2	87.5
3	81.8
4	100
5	100
6	87.5
7	70
8	66.7
9	81.8
10	66.7
11	37.5
12	100
13	87.5
14	100
15	88.9
16	60
Control	
17	70
18	70
19	63.6
20	77.8
21	50
22	80
23	44.4
24	55.6
25	75
26	54.5
27	77.8
28	63.6
29	28.6
30	100
31	50
32	70

<sup>a</sup> Calculated by dividing operated side  $\delta$  angle by nonoperated side  $\delta$  angle (i.e. the difference between resting toe flexion angle and toe flexion angle with force applied).

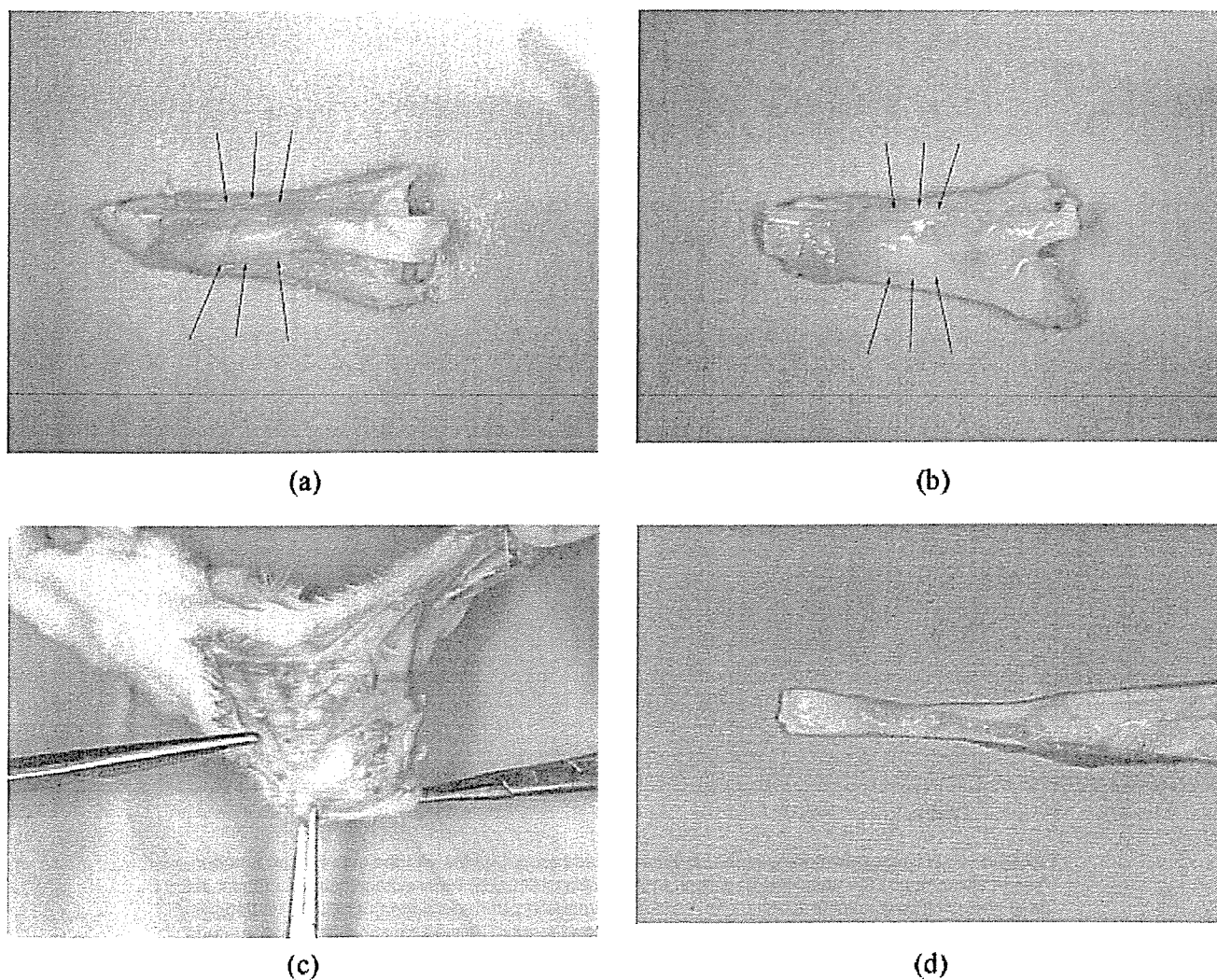


**Figure 2.** (a) Appearance of the lesion site in the control group. Degree of scar formation at the repaired tendon was greater (arrows) in the control group than in the alginate-treated group. (b) Macroscopic appearance of the lesion site in the alginate-treated group. In the alginate-treated group, the repaired tendon was surrounded by a transparent membrane (arrows). (c) Macroscopic appearance of the lesion site. A yellowish gel thought to be undissolved alginate was seen in the intact part of the sheath at week 4. (d) Macroscopic appearance of the lacerated tendon in the alginate-treated group. Repair of the tendon appeared complete.

severe contractures occurred in some animals and stable adhesion was not possible in this rabbit model. We therefore used partial lacerations in the present model to avoid the variability inherent in full-thickness lacerations.<sup>9-12</sup> Surgical procedure was based on the model used in an earlier study.<sup>9</sup>

Rabbits were anesthetized with an intravenous infusion of ketamine hydrochloride (0.5 mg/kg). After preparation of the hind limb, the skin was incised and the tendon sheath of the flexor digitorum communis muscle was exposed just above the ankle. The sheath was opened transversely and the tendon isolated. The toes were then maximally flexed and the intra-synovial part of the tendon was drawn into the wound. Using a scalpel blade, the tendon on the medial side was divided transversely as distally as possible, with the resulting lacer-

ation affecting ~50% of the volume of the structure. In 16 animals, the site of the lesion was coated with 1.0 g (by weight) of alginate paste (10% solution) (alginate group), while the remaining 16 received no such coating (control group). After surgery, the toes were placed back into the neutral position, allowing the injured portion of the tendon to slide distally to lie within an undisturbed part of the sheath. The excised sheath was not repaired and the skin was closed with 3-0 nylon. Postoperative immobilization was not applied.

#### Mechanical Evaluation

At 4 weeks postoperatively, the 16 animals in each group were killed by anesthetic overdose. Both legs were disartic-

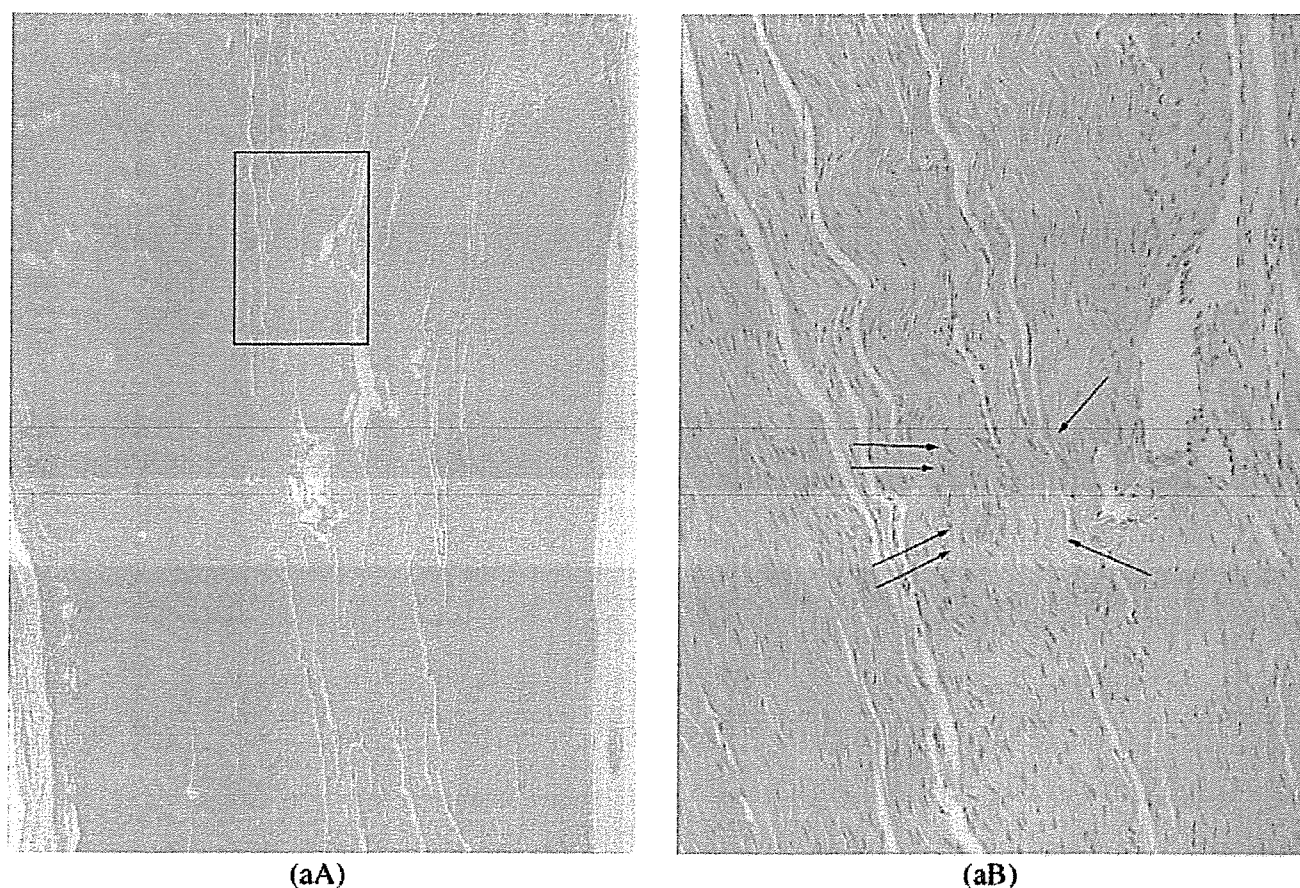


**Figure 3.** (a) Histological findings in the alginate-treated group. (A) View of the entire injured tendon. The left side shows the unlacerated portion of the tendon ( $\times 10$ ). (B) Higher magnification of the inset in (A) ( $\times 40$ ). Arrows indicate longitudinal, smooth remodeling of the collagen fibers. (b) Histological findings in the control group. (A) View of the entire injured tendon. The left side shows the unlacerated portion of the tendon ( $\times 10$ ). (B) Higher magnification of the inset in (A) ( $\times 40$ ). Arrows indicate that a random pattern of fibers was still evident.

ulated at the knee. The skin and muscles were removed, leaving the flexor digitorum tendon intact at the posterior aspect of the leg. The tendon was dissected free from its bony origin, and a pair of forceps was attached to its proximal end. The leg was observed from the medial side in front of a white screen bearing radial lines representing a protractor; lines were drawn every 10 degrees from horizontal to 360 degrees. The first metatarsophalangeal joint capsule was exposed and the head of the first metatarsal bone was positioned at the center of the protractor. The limb was placed in a vertical position with its proximal tibia immobilized by a clamp while the mid and anterior parts of the foot were left free and positioned horizontally. The posterior part of the foot, including the calcaneus, was held in another clamp. The flexion angle of the first toe was measured to the nearest 5 degrees when the proximal end of the tendon was pulled with 400 g force (measured by a spring-type scale) (Figure 1). We positioned a camera at a fixed distance from the screen and photographed the limb in the resting position and when weight was applied to the tendon. When the photographs

were developed, the flexion range of motion was determined as the difference between the resting position and the flexed position. The observer (K.S.) was blinded to the treatment each animal received. The flexion ratio was calculated by dividing the flexion angle of the surgically treated side by the angle of the nonsurgically treated side and was expressed in percentage. An unpaired *t* test was used to evaluate the differences between the treated and control groups at 4 weeks.

#### Histological Evaluation

Tendon healing, peritendinous adhesion, and the state of alginate solution remaining locally were evaluated by observing the appearance of the repaired site with the naked eye at postoperative week 4. A longitudinal section of the repaired site was stained with hematoxylin and eosin and observed microscopically to determine the amount of scar formation and to evaluate the remodeling of collagen fibers.

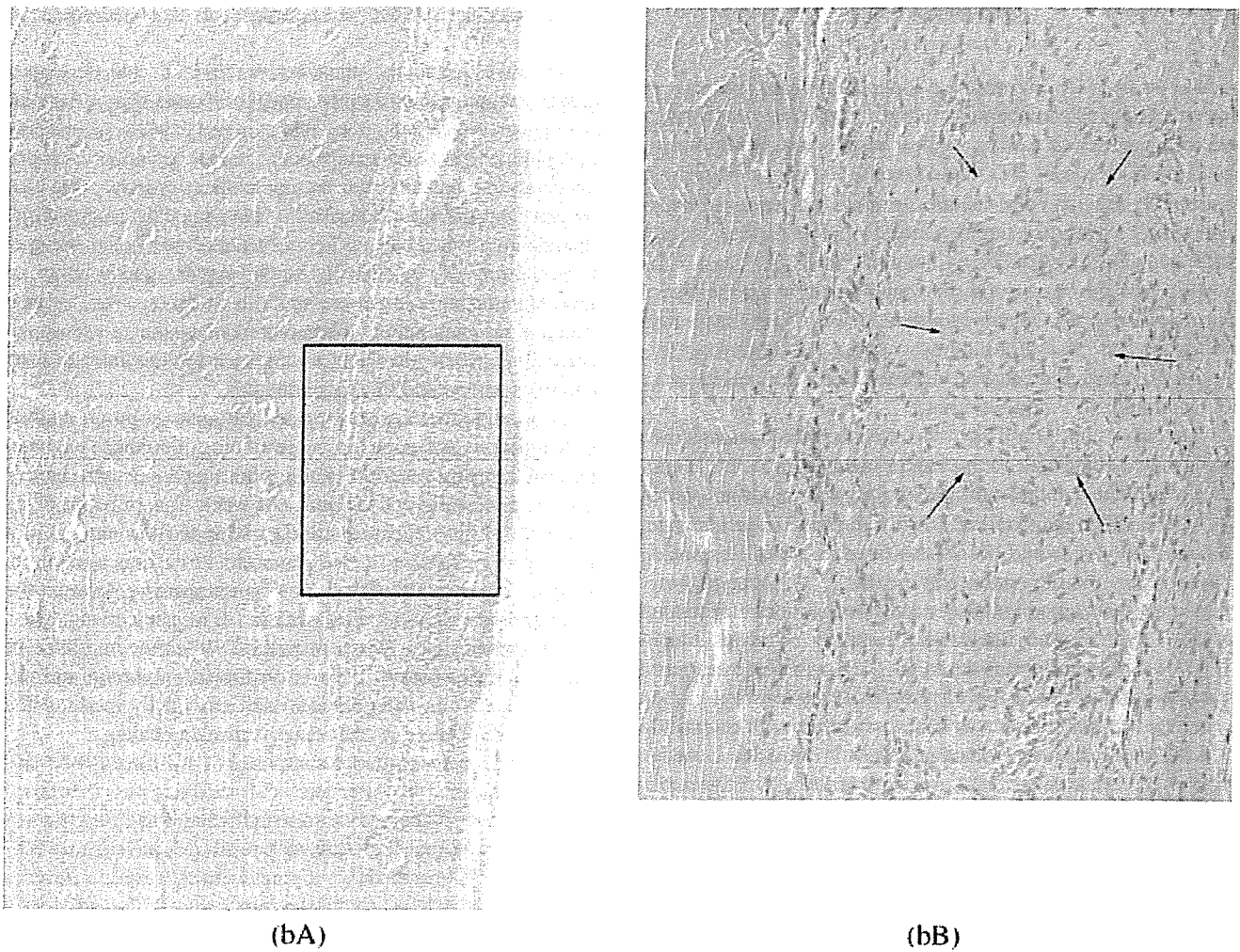


Figure 3. (continued)

## RESULTS

At 4 weeks postoperatively, the wound site had healed well in all animals. No evidence of rupture, faulty union, local inflammation, or systemic complications was observed.

### Mechanical Evaluation

Flexion ratio was significantly greater in the alginate-treated group ( $81.5 \pm 17.4$ ; SE = 4.35) than in the control group ( $64.4 \pm 17.0$ ; SE = 4.26) at 4 weeks postoperatively ( $p = 0.009$ ) (Table 1).

### Histological Evaluation

**Macroscopic Appearance of the Lesion Site.** Repair of the lacerated sites appeared complete at week 4 in both groups. The amount of scar formation at the repaired tendon

was greater in the control group than in the alginate-treated group [Figure 2(a,b)]. However, this was difficult to quantify. In the alginate-treated group, the repaired tendon was surrounded by a transparent membrane [Figure 2(b)], which was thought to be a mixture of alginate paste and the original synovial fluid. In all alginate-treated rabbits, a yellowish paste was observed within the intact sheath at the ankle at week 4, which was thought to be undissolved alginate paste [Figure 2(c)], and the tendons healed, with good appearance in terms of physical properties and luster [Figure 2(d)]. In all animals in the control group, union was attained but the original luster was lost.

**Histology.** In both groups, fibroblasts and collagenous tissue had proliferated at the repaired site. However, longitudinal well-oriented tenocytes, indicating smooth remodeling of the collagen fibers, were observed in all toes in the alginate-treated group [Figure 3(a)], whereas poorly oriented cells and a random pattern of fibers were still seen in the control group [Figure 3(b)].

## DISCUSSION

In the last decade, scientific evidence supported the theory that the extrinsic mechanism might merely be an inflammatory response to tendon injury rather than being essential to the process of tendon repair.<sup>13</sup> In an effort to minimize adhesion after tendon repair, biochemical materials such as monomolecular cellulose filter tubes,<sup>1</sup> polyethylene tubes,<sup>2</sup> and silastic sheaths<sup>3</sup> have been tested as mechanical barriers around the repair site, but no satisfactory approach has been established. All these materials failed because they stimulated a severe inflammatory response or prevented nutrient diffusion to the healing tendon, leading to tendon necrosis.

Currently, both intrinsic and extrinsic mechanisms are believed to contribute to the tendon healing process.<sup>6</sup> Tenocytes within the tendon and epitenon play an important role in the intrinsic mechanism, while in the extrinsic mechanism, inflammatory cells and fibroblasts from the overlying sheath and periphery are the main participants.<sup>13,14</sup> Although synovial sheath cells move into the tendon core soon after tendon injury,<sup>5</sup> there is a time lag in the initiation of intrinsic healing.<sup>6</sup> It is therefore considered that if an intrinsic response could be stimulated at the early stage of tendon healing, the outcome of tendon repair would be preferable with regard to reducing peritendinous adhesion. Based on this idea, a wide range of substances, including fibrin sealant,<sup>11</sup> 5-fluorouracil,<sup>12</sup> sodium hyaluronate,<sup>15</sup> aprotinin,<sup>16</sup> and TGF- $\beta$ 1 neutralizing antibody,<sup>17</sup> have been experimentally applied to the tendon repair, with the aim of reducing extrinsic healing and stimulating the intrinsic mechanism. However, problems such as high cost of raw materials, potential side effects, and limited bioavailability have prevented widespread clinical use of these agents.<sup>17</sup>

We have accordingly focused our attention on alginate, a natural biodegradable material, rather than on the development of synthetic pharmacologic substances.

Recently, alginate has been used as a wound dressing material and as a food additive on account of its high viscosity and good biocompatibility.<sup>7</sup> It is also used extensively in cell encapsulation and tissue engineering because of its easy gelation, good biocompatibility, and low toxicity.<sup>7,18</sup> The best results have been obtained with alginate microcapsules in the field of allo- and xenogenic islet transplantation.<sup>8</sup> In cell encapsulation, alginate gel that is crosslinked with covalent bonds is generally applied. However, this has a hard consistency, making it unsuitable for application as a coatable or injectable tendon adhesion barrier gel. To create alginate with adequate handling properties, we developed a technique involving very high concentrations of sodium alginate without using the crosslinking method. As high-molecular-weight alginate chains in this formulation adopt very coiled configurations in solution, we considered that this results in alginate occupying a large volume for its mass and acting as a sieve for molecules and cells passing through the solution. Ideally, such a configuration would allow permeation of molecules such as oxygen, glucose, insulin, and other nutrients of

small molecular size that are necessary for cells and organs to survive.

We investigated the antiadhesive effect of the developed alginate solution using a rabbit model of tendon injury. At week 4, the most critical time after tendon surgery, tendon repair was not inhibited, and statistically better tendon excursion was obtained in the alginate-treated group. Macroscopically, alginate remained in the sheath at week 4. Histologically, longitudinal remodeling of the collagen fibers was observed in the alginate-treated group. No evidence of tendon rupture, faulty union, or local inflammation was observed. This suggests that alginate solution has no inhibitory effect on tendon healing and does not cause foreign body reaction, as confirmed in the fields of food additives and wound dressing materials.<sup>7</sup>

A possible mechanism by which alginate solution inhibits peritendinous adhesions is by providing a suitable environment for intrinsic tendon healing, both as a selective barrier and as a cell delivery medium. At week 4, as a result of its adhesive ability, alginate solution wrapped the tendon in a manner very similar to that observed in cell encapsulation. Instilled alginate solution works by interposing between the lacerated tendon and the injured sheath as a selective barrier, thereby avoiding early scar formation. When the migration of extrinsic inflammatory cells is obstructed, epitenon and endotenon cells from the tendon itself can easily move to the lacerated site, thereby facilitating intrinsic healing.

Alginate is a copolymer composed of 1,4-linked  $\beta$ -D manuronic acid and  $\alpha$ -L-gluronic acid residues, has a carboxyl base ( $-\text{COO}^-$ ) attached to its branch chain, and functions as a polyanion polymer that attracts positive ions such as  $\text{Na}^+$  and  $\text{Ca}^{2+}$ .<sup>7</sup> Consequently, alginate attracts water, forms a hydrogel, and swells around the repair site. It also provides a suitable environment for diffusion and transportation of certain nutrients.<sup>18</sup>

Both the low cost of production and bioabsorbability of alginate may render it very useful in the clinical setting. Because all species of brown seaweed contain the source molecule algin, alginate is abundant enough to be used commercially.<sup>7</sup> Alginate is largely produced in the food industry as a stabilizer in ice cream and as a thickener in fruit drinks.<sup>7</sup> Although usually hydrolyzed by alginate lyase in brown seaweed, alginate takes longer to be hydrolyzed in the human body because humans lack the appropriate hydrolyzing enzyme.<sup>7</sup> Alginate therefore remains for several weeks at the repair site, a great advantage considering the time frame of tendon healing. Hyaluronate, which is also a biodegradable mucopolysaccharide and well known as one of the main components of synovial fluid, has also been used experimentally to prevent peritendinous adhesion.<sup>15</sup> However, in contrast to alginate, hyaluronate is rapidly broken down in the human body by hyaluronidase and disappears within 72 h.<sup>19</sup>

In summary, the results of the present study suggest that alginate solution is an effective material for inhibition of peritendinous adhesion, and that its application represents a promising approach for treating tendon injury. Although alginate solution showed a favorable antiadhesive effect in our

rabbit tendon model, further studies are required to determine suitable concentration and viscosity in clinical use.

### REFERENCES

- Ashley FL, Stone RS, Alonso-Artied M, Syverud J, Edwards JW, Sloan RF, Mooney SA. Experimental and clinical studies on the application of monomolecular cellulose filter tubes to create artificial tendon sheath in digits. *Plast Reconstr Surg* 1959;23:526-534.
- Gonzales RI. Experimental tendon repair within the flexor tunnels. Use of polyethylene tubes for improvement of functional results in the dog. *Surgery* 1949;26:181-198.
- Stark HH, Boyes JH, Johnson L, Ashworth CR. The use of paratenon, polyethylene film, or silastic sheeting to prevent restricting adhesions to tendons in the hand. *J Bone Joint Surg Am* 1977;59:908-913.
- Amadio PC. Tendon and ligament. In: Cohen KI, Diegelmann RF, Lindblad WI, editors. *Wound Healing: Biochemical and Clinical Aspects*. Philadelphia: Saunders; 1992. pp 384-396.
- Harrison RK, Mudera V, Grobbelaar AO, Jones ME, McGrouther DA. Synovial sheath cell migratory response to flexor tendon injury: An experimental study in rats. *J Hand Surg Am* 2003;28:987-993.
- Khan U, Ocleston NL, Khaw PT, McGrouther DA. Differences in proliferative rate and collagen lattice contraction between endotenon and synovial fibroblasts. *J Hand Surg Am* 1998;23:266-273.
- Skjak-Braek G. Alginates: Biosyntheses and structure-function relationships relevant to biomedical and biotechnological applications. *Biochem Soc Trans* 1992;20:27-33.
- Mullen Y, Maruyama M, Smith CV. Current progress and perspectives in immunoisolated islet transplantation. *J Hepatobiliary Pancreat Surg* 2000;7:347-357.
- Merle M, Dautel G, Medinaceli L. Inhibition of peritendinous adhesions by ADCON-T/N in a rabbit flexor tendon model. In: Vastamaki M, Vilkki S, Goransson H, Jaroma H, Raatikainen T, Viljakka T, editors. *The Sixth Congress of IFSSH*. Bologna, Italy: Monduzzi Editore; 1995. pp 1025-1028.
- Thomas SC, Jones LC, Hungerford DS. Hyaluronic acid and its effect on postoperative adhesions in the rabbit flexor tendon. A preliminary look. *Clin Orthop Relat Res* 1986;206:281-289.
- Frykman E, Jacobsson S, Widenfalk B. Fibrin sealant in prevention of flexor tendon adhesions: An experimental study in the rabbit. *J Hand Surg Am* 1993;18:68-75.
- Akali A, Khan U, Khaw PT, McGrouther DA. Decrease in adhesion formation by a single application of 5-fluorouracil after flexor tendon injury. *Plast Reconstr Surg* 1999;103:151-158.
- Jalilaj M. Advances in the biology of zone II flexor tendon healing and adhesion formation. *Ann Plast Surg* 2000;45:83-92.
- Chang J, Most D, Stelnicki E, Siebert JW, Longaker MT, Hui K, Lineaweaver WC. Gene expression of transforming growth factor  $\beta$ -1 in rabbit zone II flexor tendon wound healing: Evidence for dual mechanisms of repair. *Plast Reconstr Surg* 1997;100:937-944.
- Hagberg L, Sweden M, Gerdin B. Sodium hyaluronate as an adjunct in adhesion prevention after flexor tendon surgery in rabbits. *J Hand Surg Am* 1992;17:935-941.
- Komurcu M, Akkus O, Basbozkurt M, Gur E, Akkus N. Reduction of restrictive adhesions by local aprotinin application and primary sheath repair in surgically traumatized flexor tendons of the rabbit. *J Hand Surg Am* 1997;22:826-832.
- Chang J, Thunder R, Most D, Longaker MT, Lineaweaver WC. Studies in flexor tendon wound healing: Neutralizing antibody to TGF- $\beta$ 1 increases postoperative range of motion. *Plast Reconstr Surg* 2000;105:148-155.
- Smidsrod O, Skjak-Braek G. Alginate as immobilization matrix for cells. *Trends Biotechnol* 1990;8:71-78.
- Wigren A, Wik O, Falk J. Repeated intraarticular implantation of hyaluronic acid. An experimental study in normal and immobilized adult rabbit knee joints. *Ups J Med Sci Suppl* 1975;17:1-20.



Takashi Kitamura · Jun Hashimoto ·  
Tsuyoshi Murase · Tetsuya Tomita · Takako Hattori ·  
Hideki Yoshikawa · Kazuomi Sugamoto

## Radiographic study of joint destruction patterns in the rheumatoid elbow

Received: 7 January 2006 / Revised: 1 April 2006 / Accepted: 3 April 2006  
© Clinical Rheumatology 2006

**Abstract** Knowledge of the pattern of joint destruction is important for planning the therapeutic approach to rheumatoid arthritis (RA) of the elbow. Accordingly, we carried out a large-scale radiographic study with the objective of elucidating the joint destruction pattern in rheumatoid elbows. From 2001 through 2003, we examined and took plain X-rays of both elbows of 193 RA patients (i.e., 386 elbows), consisting of 18 men and 175 women, with a mean age of 57.0 years. Radiographic images of the elbow joints were used to classify the degree of bone loss in various zones on the elbow joint surface into four grades of severity, and joint destruction was compared between the left and right elbows. In addition, correlation in the extent of bone loss between each of the zones of the same elbow and differences in the extent of bone loss were analyzed statistically. The results showed direct correlations for destruction of the elbow joint surface among the zones for the left and right elbow joints and in the same elbow joint. However, more severe destruction was observed on the radial side of the humeral trochlea, and it was surmised that destruction of the elbow joint must begin at that site and gradually spread mediolaterally. In addition, in the same elbow joint, the correlation in the degree of bone loss between the trochlea of humerus and the trochlear notch

was especially strong, indicating that the bone destruction at both sites represented mirror lesions. We conclude that when performing radiographic diagnosis of the joint damage in the rheumatoid elbow, knowledge of this pattern of joint destruction will be useful for assessing whether there is joint destruction in the initial stage and for deciding the therapeutic approach.

**Keywords** Elbow joint · Radiography · Rheumatoid arthritis

### Introduction

The elbow joint is a common site for the development of rheumatoid arthritis (RA), and it is one of the most important joints in the upper limb as it controls the reach of the hand [1–4]. For this reason, disorders of the elbow joint can seriously interfere with activities of daily living (ADL) of RA patients. In general, when arthropathy is mild, therapy consists of conservative treatments such as drug administration and/or intraarticular injection of steroid. In severe disease, surgical treatments such as synovectomy and artificial elbow joint replacement may be performed [1–4]. For treatment selection and planning, it is very important for the physician to have a good understanding of the pattern of destruction that has occurred in the RA elbow joint. However, it is unfortunate that to date very few reports of analysis of the pattern of bone destruction in RA elbow joints have been published.

We therefore carried out a large-scale radiographic study with the objective of elucidating the pattern of RA elbow joint bone destruction.

### Subjects

From 2001 to 2003, we examined plain X-rays of both elbow joints of 233 patients who satisfied the ARA diagnostic criteria. Forty of these patients were excluded from the present study due to previous synovectomy or

T. Kitamura (✉)  
Department of Orthopedic Surgery, Kaizuka City Hospital,  
3-10-20, Hori, Kaizuka,  
Osaka 597-0015, Japan  
e-mail: kitamura@tb3.so-net.ne.jp  
Tel.: +81-0724-225865  
Fax: +81-0724-396061

J. Hashimoto · T. Murase · T. Tomita ·  
H. Yoshikawa · K. Sugamoto  
Department of Orthopaedics,  
Osaka University Medical School,  
2-2, Yamadaoka, Suita,  
Osaka 565-0871, Japan

T. Hattori  
Department of Orthopedic Surgery, NTT West Osaka Hospital,  
2-6-40, Karasugatsuji, Tennouji,  
Osaka 543-8922, Japan

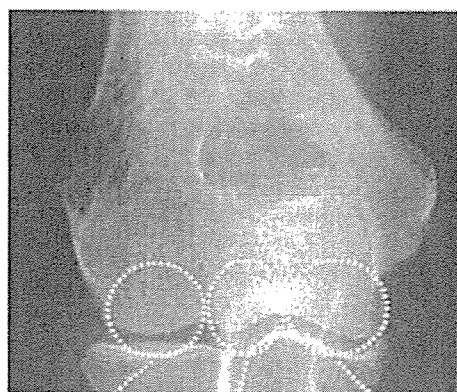
artificial elbow joint replacement (33 patients) or because the X-rays were unreadable (seven patients). The remaining 193 RA patients, i.e., 386 elbows, were the subjects of this study. They consisted of 18 men and 175 women, with an age range of 23~84 years (mean 57.0 years). History of drug administration, including steroids, and duration of RA were unclear.

## Methods

Radiographic classification of the severity of RA was performed on the basis of plain X-ray anteroposterior images and lateral images of the bilateral elbow joints that were obtained for each patient at the time of final examination. X-rays were taken with the patient in a sitting position. Frontal views were obtained with the elbow joint extended and the forearm in the supine position, while lateral views were obtained with the elbow joint flexed at 90° and the forearm in the intermediate position. The frontal images were divided into three zones: the capitulum of the humerus (zone A), the radial side of the humeral trochlea (zone B), and the ulnar side of the humeral trochlea (zone C). The extent of destruction of the joint surface was determined for each of these zones. In addition, from the lateral view, the extent of joint surface destruction was determined for the olecranon (zone D).

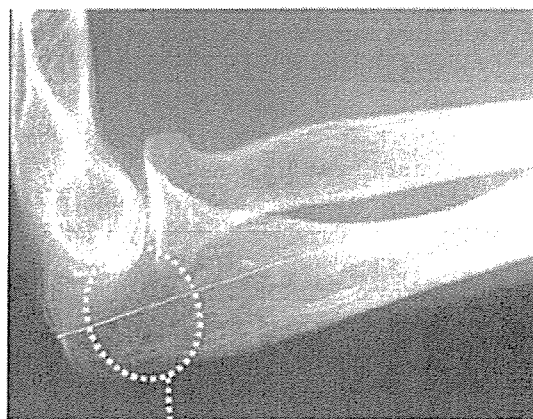
Extent of joint destruction was assessed by reference to a template of the normal elbow joint that had been prepared in advance. The ratings used were grade 0, no bone loss; grade 1, less than 3 mm of bone loss from the joint surface; grade 2, bone loss of 3 to less than 6 mm; and grade 3, bone loss of 6 or more mm (Figs. 1 and 2).

We investigated the extent of bone destruction observed in each of the joint zones, and also investigated whether there was any correlation in destruction among the zones. In practice, we first investigated the correlation in the extent of bone loss in the same zone in both elbows of the same patient, and then compared joint destruction in the left and



**zone A** Capitulum  
**zone B** Radial side of trochlea  
**zone C** Ulnar side of trochlea

Fig. 1 Radiographic classification (zones A, B, and C)



**zone D**  
**Olecranon**

Fig. 2 Radiographic classification (zone D)

right elbows. In addition, the correlation in the extent of bone loss among each zone of the same elbow and differences in the extent of bone loss were analyzed statistically.

Spearman's ranked correlation coefficients were used for statistical analyses of correlations, while one-way analysis of variance (ANOVA) and Fisher's least significant difference (LSD) test were used to analyze differences in extent of bone loss.

## Results

The extent of bone loss in each zone of the joint as seen on frontal X-ray images was as follows: zone A, 26.2% grade 0, 62.1% grade 1, 8.8% grade 2, and 2.8% grade 3; zone B, 26.2% grade 0, 37.0% grade 1, 26.9% grade 2, and 9.8% grade 3; and zone C, 26.9% grade 0, 62.1% grade 1, 2.6% grade 2, and 8.3% grade 3. The extent of bone loss was therefore similar in zone A and zone C, whereas zone B exhibited a lower percentage rated as grade 2 and a higher percentage rated as grade 3 compared with the other two zones. The extent of bone loss seen on lateral X-ray images (zone D) was grade 0 in 27.2%, grade 1 in 61.1%, grade 2 in 8.3%, and grade 3 in 3.4% (Table 1).

A significant correlation was found for the extent of bone loss in the same zone between the left and right elbows, and correlation was found for bilateral elbow joint destruction (zone A  $r=0.833$ ,  $p<0.001$ ; zone B  $r=0.804$ ,  $p<0.001$ ; zone C  $r=0.881$ ,  $p<0.001$ ; and zone D  $r=0.887$ ,  $p<0.001$ ).

In addition, statistically significant correlations were also found for the extent of bone loss among zones in the same elbow ( $r=0.789\sim0.951$ ,  $p<0.001$ ) (Fig. 3). A particularly strong correlation was demonstrated between zone C and zone D ( $r=0.951$ ,  $p<0.001$ ).

On the other hand, the extent of bone loss was significantly greater in zone B compared with zone A and zone C ( $p<0.05$ ), indicating that joint surface

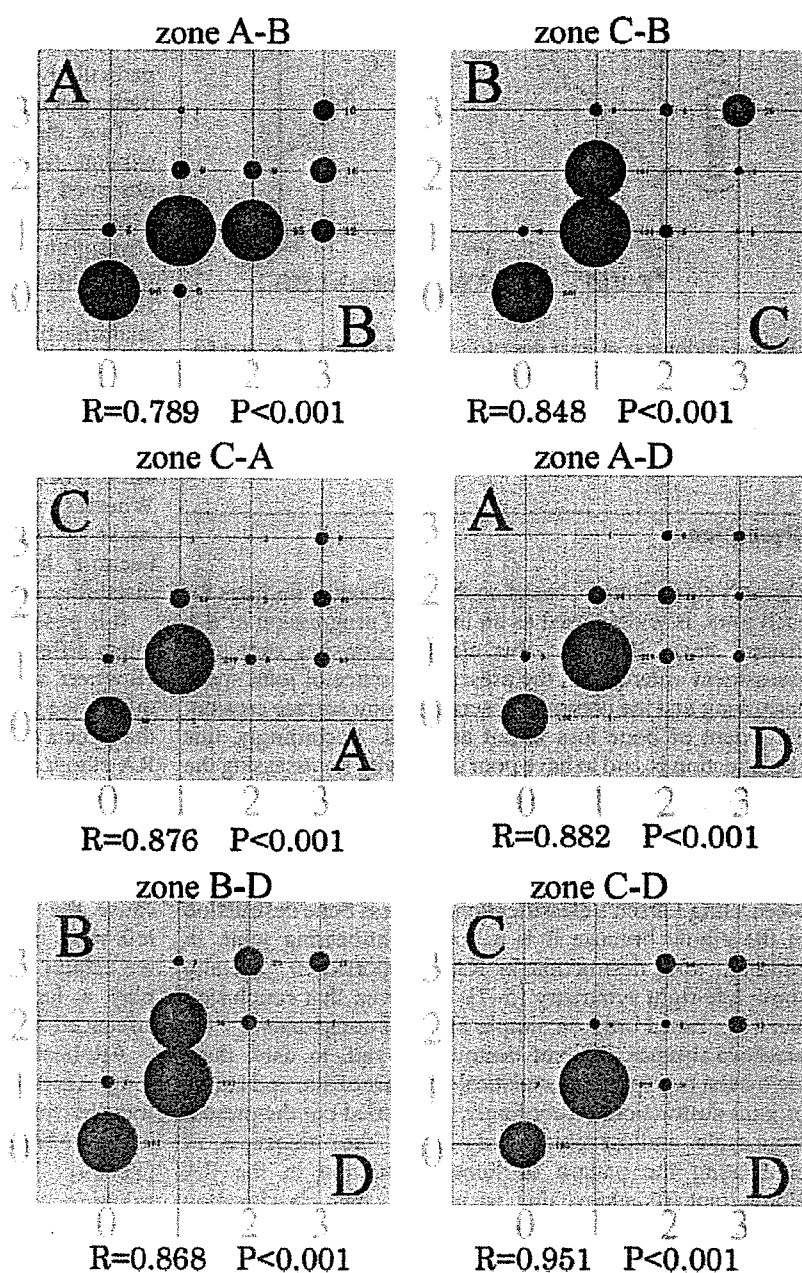
**Table 1** Radiographic classification of severity of joint destruction in the elbow ( $n=193$ )

Grade	Zone A		Zone B		Zone C		Zone D	
	R/L	Total(%)	R/L	Total(%)	R/L	Total(%)	R/L	Total(%)
0	50/51	26.2	49/52	26.2	51/53	26.9	51/54	27.2
1	123/117	62.2	73/70	37.1	120/120	62.2	117/119	61.1
2	14/20	8.8	54/50	26.9	7/3	2.6	16/16	8.3
3	6/5	2.8	17/21	9.8	15/17	8.3	9/4	3.4
Total	193/193	100	193/193	100	193/193	100	193/193	100

destruction was more advanced in the central part of distal humerus articular surface than at other sites (Fig. 4).

In addition, bone destruction of the humeral trochlea that extended to the olecranon fossa, i.e., a so-called Y-shaped

**Fig. 3** Correlation of joint destruction among zones A, B, C, and D (386 joints)



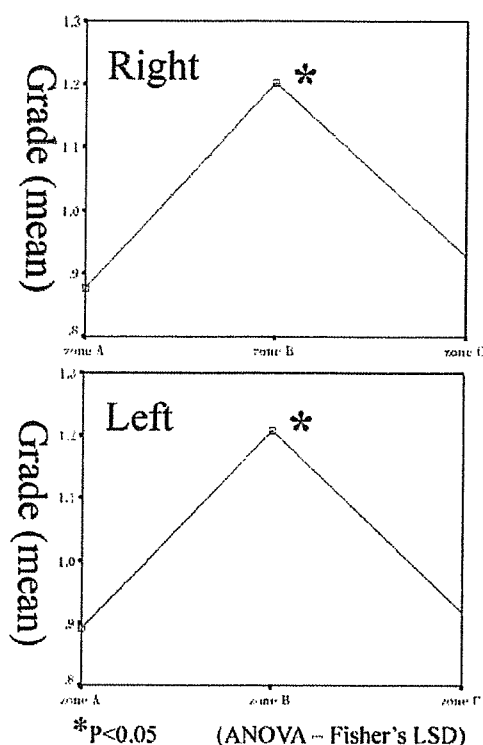


Fig. 4 Distribution of joint destruction grade (zones A, B, and C)

deformity, was observed in six of the patients, although this was bilateral in only two patients.

## Discussion

Larsen's classification, based on the radiological findings for each joint, is widely used as an index of progression of RA disease stage. However, this classification has only two assessment criteria, i.e., the presence/absence of joint space narrowing and the presence/absence of joint surface erosion; the extent of bone loss is not assessed. Accordingly, this classification is said to have poor sensitivity for assessing the extent of joint destruction [5–7]. Lehtinen et al. [7] reported that joint space narrowing in the RA elbow differs from that in weight-bearing joints in that it occurs only subsequent to erosive destruction. They also stated that caution is necessary when using Larsen's classification to assess bone destruction in the elbow because it is a nonweight-bearing joint. In addition, joint destruction in RA is reported to generally show left–right symmetry [5–7]. However, that conclusion has been based only on simple bilateral comparison of the presence/absence of joint destruction, and, to date, there have been no reports of statistical analysis of site and extent of joint destruction. Accordingly, we carried out the present large-scale radiographic study with the objective of elucidating the pattern of bone destruction in the RA elbow joint. To achieve this, we used our own classification system to assess the extent of bone loss in various zones on the elbow joint surface, and joint destruction was compared

between the left and right elbows. We then performed statistical analyses to determine whether there were any correlations in the extent of bone loss among each of the zones in the bilateral elbows and in the same elbow.

Our patients showed positive correlations among each of the zones for the extent of bone loss in the same elbow joint, and positive correlations were also found for the extent of joint surface bone loss in the same zones in the bilateral elbows. On the other hand, when we investigated the extent of bone loss in each zone in the same joint, we found it to be significantly greater on the radial side of the humeral trochlea compared with the ulnar side of the trochlea and the capitulum. We therefore surmised that the joint destruction must begin at the radial side of the humeral trochlea and gradually spread mediolaterally. In addition, in the same elbow joint, the correlation in the degree of bone loss between the ulnar side of the trochlea and the olecranon was particularly strong, indicating that the bone destruction at both sites represented symmetrical lesions.

Two theories have been proposed in an attempt to explain the underlying mechanism of the destruction observed in upper limb joints with RA. In the first, the principal cause is considered to be destruction and absorption of cartilage and bone as a result of the actions of cytokines released from the synovial tissue [8, 9]. The second theory holds that the major effects arise from anatomical and/or mechanical factors [10]. Ochi et al. [11] reported that even in the same joint the mechanism of destruction varies widely depending on the disease type. That is, they found that in the type involving damage to the smaller joints, the main bone destruction consisted of erosion of the joint surface due to proliferation of synovitis. Whereas with the mutilating type of arthritis, the main cause of bone destruction was crushing of bone that had become highly osteoporotic because of severe joint instability due to joint laxity.

It is possible that the level of stress applied to the elbow joints differs between the dominant and nondominant arm. However, in the present study, we found no clear left–right difference in the extent of joint destruction, suggesting that the effects of mechanical factors on bone destruction in the RA elbow are slight. Even so, consideration must be given to the fact that most of the patients in our present series were at an earlier stage of the disease, showing a milder degree of joint destruction. Conversely, however, some patients with severe joint destruction, such as is likely to cause the so-called Y-shaped deformity, exhibited clear left–right differences in the extent of damage. Therefore, we cannot rule out the possibility that mechanical factors play a larger role than immunological factors in the advanced stages of joint destruction.

Application of axial compression in the direction of the long axis of the forearm reportedly results in almost equal transmission of the force to the radial joint and the ulnar joint, or slightly greater transmission to the radial joint [12–14]. The surface of the radial side of the humeral trochlea becomes the varus–valgus pivot point of the elbow [15], and for this reason it is possible that when joint laxity occurs due to synovitis, forces are concen-